Pure Appl. Chem., Vol. 81, No. 8, pp. 1357–1383, 2009.
doi:10.1351/PAC-CON-08-07-20

Interplay between spin crossover and exchange interaction in iron(III) complexes*

Roman Boča[1,‡], Ivan Nemec[1], Ivan Šalitroš[1], Ján Pavlik[1], Radovan Herchel[2], and Franz Renz[3]

[1]Institute of Inorganic Chemistry, Slovak University of Technology (FCHPT), SK-812 37 Bratislava, Slovakia; [2]Department of Inorganic Chemistry, Palacký University, CZ-77147 Olomouc, Czech Republic; [3]Institute of Inorganic Chemistry, Leibniz University Hannover, D-30167 Hannover, Germany

Abstract: In the dinuclear and polynuclear metal complexes exhibiting the low-spin (LS) to high-spin (HS) transition, the spin-crossover phenomenon interferes with the magnetic exchange interaction. The latter manifests itself in forming spin-multiplets, which causes a possible overlap of the band originating in different reference spin states (LL, LH, HL, and HH). A series of dinuclear Fe(III) complexes has been prepared; the iron centers are linked by a bidentate bridge (CN^-, and diamagnetic metallacyanates $\{Fe(CN)_5(NO)\}$, $\{Ni(CN)_4\}$, $\{Pt(CN)_4\}$, and $\{Ag(CN)_2\}$). Magnetic measurements confirm that the spin crossover proceeds on the thermal propagation. This information has been completed also by the Mössbauer spectral (MS) data. A theoretical model has been developed that allows a simultaneous fitting of all available experimental data (magnetic susceptibility, magnetization, HS mole fraction) on a common set of parameters.

Keywords: Fe(III) complexes; magnetism; spin crossover; exchange interaction; Mössbauer spectra.

INTRODUCTION

Spin crossover (spin transition) can be viewed as a unimolecular reaction upon which the low-spin (LS) entities (molecular complexes, chains, or networks) are transformed to the high-spin (HS) species primarily by heating. The conversion from LS to HS states is an entropy-driven reaction: with $\Delta S > 0$ and $\Delta H \sim kT > 0$, there exists a critical temperature $T_c = \Delta H/\Delta S$ above which the conversion proceeds spontaneously. The degree of the conversion is characterized by the temperature dependence of the HS mole fraction, x_H, which defines the equilibrium constant $K = x_H/(1 - x_H)$. In an ideal case, the van't Hoff formula is obeyed, i.e., $\ln K$ vs. $1/T$ is a linear function [1].

The spin crossover in mononuclear complexes is a case of an electron bistability, associated with the existence of two minima (L and H) of the Gibbs energy [2]. The separation of the reference states is $\Delta_1 = E(H) - E(L) \sim \Delta H$. The spin conversion is usually schematized on the basis of the orbital diagram, as shown in Fig. 1, for mononuclear Fe(III) complexes. The orbital picture, however, is a strongly oversimplified view as it abstracts from the interelectron repulsion and spin-orbit coupling.

*Paper based on a presentation at the 8th Conference on Solid State Chemistry, 6–11 July 2008, Bratislava, Slovakia. Other presentations are published in this issue, pp. 1345–1534.

‡Corresponding author

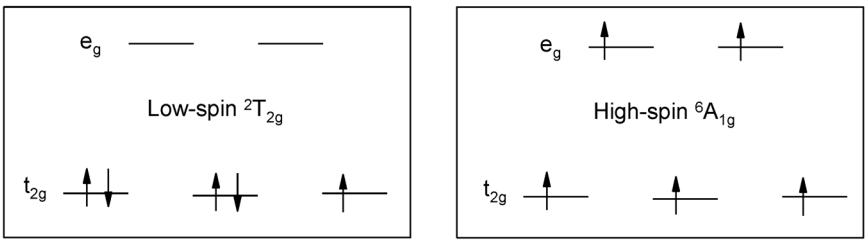

Fig. 1 Orbital picture differentiating between the LS and HS Fe(III) octahedral complexes.

The explicit inclusion of the interelectron repulsion means that atomic terms $|\alpha,L,S,M_L,M_S\rangle$ are accounted for in the orbital-spin basis set and in the language of the crystal-field (CF) theory, the CF terms $|\alpha,\Gamma,\gamma,S,M_S\rangle$ (like $^2T_{2g}$, $^6A_{1g}$). On including the spin–orbit interaction, we arrive at the CF multiplets $|\alpha,\Gamma',\gamma\rangle$ which are classified in terms of irreducible representations of the respective double group (Γ_1 through Γ_8 for **O'**). The splitting of the isolated $^2T_{2g}(\times 6)$ CF term into $\Gamma_8 = U_{3/2}(\times 4)$ and $\Gamma_7 = E_{5/2}(\times 2)$ multiplets equals $(3/2)\lambda = (3/2)\xi = 690$ cm^{-1} for Fe(III), and thus it is rather high, whereas no splitting of the term $^6A_{1g} \rightarrow (\Gamma_8, \Gamma_7)$ occurs in the first order for an octahedral system.

A theoretical modeling based upon the generalized CF theory has been done, where the electron repulsion (Racah parameters $B = 1122$ cm^{-1}, and $C = 4.2\ B$), CF strength (F_4-poles of individual ligands), spin–orbit interaction (coupling constant $\xi = 460$ cm^{-1}), orbital–Zeeman, and spin–Zeeman interactions are explicitly included [3]. The calculated Zeeman levels enter the partition function from which the magnetization and magnetic susceptibility are evaluated by using apparatus of the statistical thermodynamics. Calculated temperature dependence of the effective magnetic moment is displayed in Fig. 2, and one can see that the spin crossover occurs only in a very narrow interval of the CF strength. With $F_4 = 17\,700$ cm^{-1}, the ground CF term is $^6A_{1g}$ (HS), whereas with $F_4 = 18\,200$ cm^{-1}, it is $^2T_{2g}$ (LS). In the intermediate CF strength, a delicate situation occurs. With $F_4 = 18\,000$ cm^{-1}, the ground CF term is $^6A_{1g}$, preventing the spin crossover since it is already HS. However, the spin-orbit splitting of the excited $^2T_{2g}$ term (690 cm^{-1}) is greater than the inter-term gap (425 cm^{-1}) so that the ground CF multiplet is $\Gamma_7(\times 2) \leftarrow {}^2T_{2g}$. Therefore, the condition for the spin crossover $\Delta S > 0$ is fulfilled, and it proceeds according to the bold curve shown in Fig. 2. (Because of the calculations in the complete 252-member basis set spanned by d^5 functions, the second-order interaction of the lowest Γ_8–Γ_8 and Γ_7–Γ_7 multi-

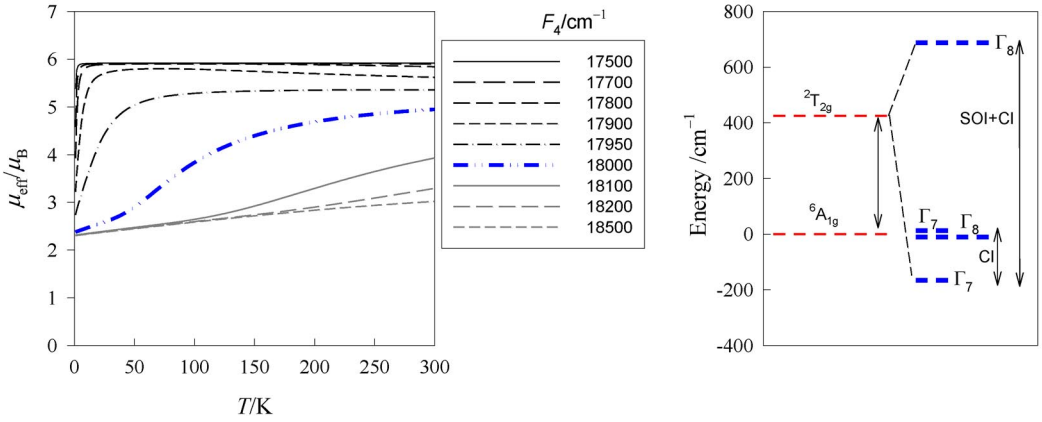

Fig. 2 Calculated temperature dependence of the effective magnetic moment for a series of octahedral Fe(III) complexes possessing different CF strengths $F_4 = 6(Dq)$. Right: energies of the lowest CF multiplets for $F_4 = 18\,000$ cm^{-1}.

plets is naturally involved.) The above modeling shows that the situation in mononuclear Fe(III) complexes is much more complex than reported so far: instead of a single energy gap, we have to consider two gaps.

In dinuclear complexes, three spin pairs could exist: LL, LH, and HH (on ignoring the intermediate-spin states, and a difference between LH and HL). The corresponding energies are separated at least by two gaps, Δ_1 (LL to LH) and Δ_2 (LH to HH). It is not implied, however, that the LH pair lies in-between LL and HH (Fig. 3). Which energy order is actually present is given by the orbital angular momentum dictated predominantly by the CF, and not by the spin angular momentum alone.

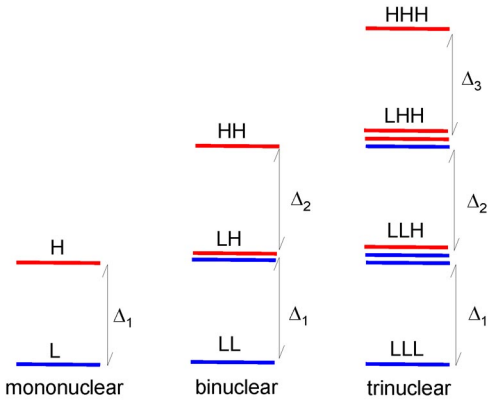

Fig. 3 Manifold reference states in polynuclear complexes exhibiting the spin crossover.

A new aspect met in dinuclear systems is the magnetic exchange interaction owing to which energy levels of the given reference state are split into a set of spin-multiplets. The bands formed in this way could be well separated, or somehow overlapping (Fig. 4). In the first case, we classify the systems to the group A/HH and A/LL, respectively, when the ground reference state is HH or LL. The members of the A/LL group are candidates for the spin crossover, whereas A/HH-type systems stay HS over the whole temperature range. In the case of overlapping bands, we use a classification to the groups B/HH and B/LL, respectively, depending on which reference state (HH or LL) is lower in energy. Group B/LL could show the spin crossover, but owing to the thermally accessible HS multiplets, the system could show in Mössbauer spectra (MS) "a residual high-spin mole fraction" even at the liquid-helium temperature. Group B/HH stays HS, but near room temperature an admixture from the LL pairs could be detected in MS. The situation becomes even more complex because of the presence of the LH state, and one cannot exclude from consideration the intermediate-spin states IL, II, and IH for low-symmetry coordination polyhedra. Moreover, the exchange coupling could be either antiferromagnetic or ferromagnetic, giving rise to the multiplet reversal. Last but not least, the spin-orbit coupling splits the reference states as argued above.

The usual assumption in the literature is that the LH state (equivalent to the HL one) is positioned in-between LL and HH states. We met an unprecedented, unsymmetrical situation, when the LH state is close to the ground state but its counterpart HL is not populated until room temperature.

Mononuclear spin-crossover systems are documented by dozens of examples, and an important piece of information has already been comprehensively reviewed [4]. Dinuclear spin-crossover systems have been studied over a longer period although systematic studies appeared only recently [5–10]. The interference of the magnetic exchange interaction with the spin-crossover phenomenon is not completely understood so far. In the tetranuclear complex $[Cr^{III}(CN)_6\{Fe^{III}L^5\}_3]$, the spin crossover proceeds among three peripheral Fe(III) centers, and the central Cr(III) atom is involved in the magnetic exchange [11]. A couple of tetranuclear Fe(II) complexes showing the spin crossover has been reported

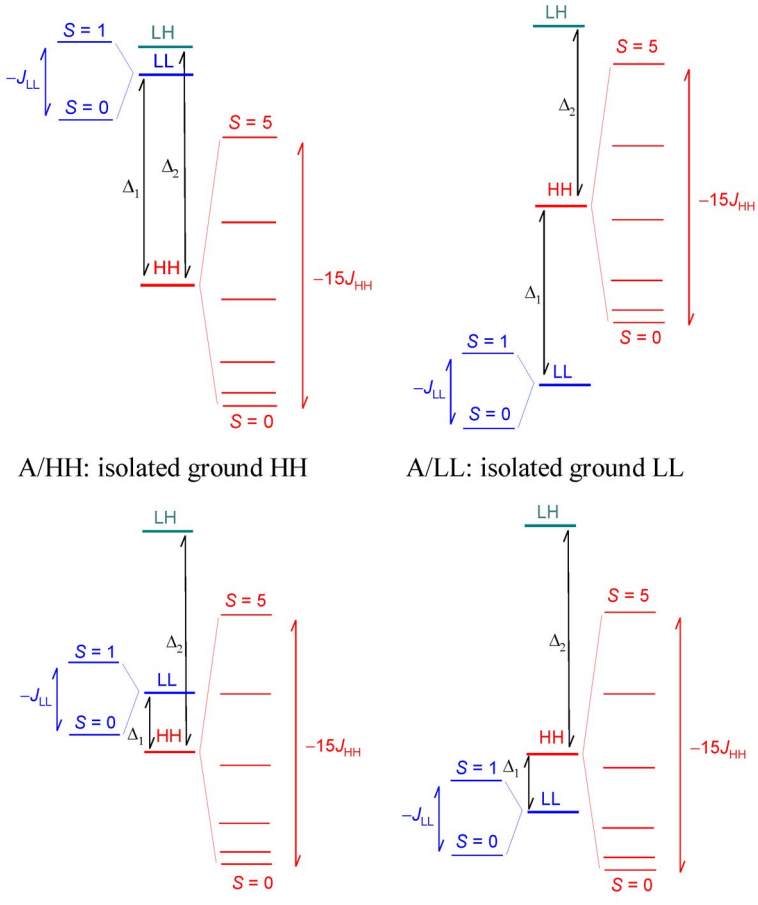

Fig. 4 Basic classes of the spin-crossover systems for dinuclear Fe(III) complexes.

[12,13]. In the heptanuclear complex $[\{Fe^{II}(CN)_6\}\{Fe^{III}L^5\}_6]Cl_2$, the central ferrocyanide unit is magnetically silent although the peripheral Fe(III) centers alter the spin state [14]. The spin crossover has been detected also in heptanuclear $[\{Co^{III}(CN)_6\}\{Fe^{III}L^5\}_6]Cl_3$ and nonanuclear $[\{Mo^{IV}(CN)_8\}\{Fe^{III}L^5\}_8]Cl_4$ complexes [15], as well as in a dodecanuclear complex with the central $\{(NC)_5Fe^{II}(CN)Co^{III}(CN)_5\}^{6-}$ unit and 10 peripheral $\{Fe^{III}L^5\}$ caps [16].

EXPERIMENTAL

Synthesis

The synthetic route for the polynuclear complexes under the investigation involves three stages: (i) Schiff condensation resulting in a pentadentate blocking ligand L^5; (ii) complexation with Fe(III) salts yielding a mononuclear precursor $[Fe^{III}L^5X]$; (iii) preparation of the dinuclear and trinuclear complexes from mononuclear building blocks.

The Schiff condensation of (substituted) *o*-salicylaldehyde with a number of aliphatic amines $H_2N(R_1)NH(R_2)NH_2$ [*det*: 1,5-diamino-3-azapentane, *pet*: 1,6-diamino-4-azahexane, *dpt*: 1,7-diamino-4-azaheptane] at a ratio of 2:1 resulted in pentadentate ligands (yellow oils) according to Scheme 1.

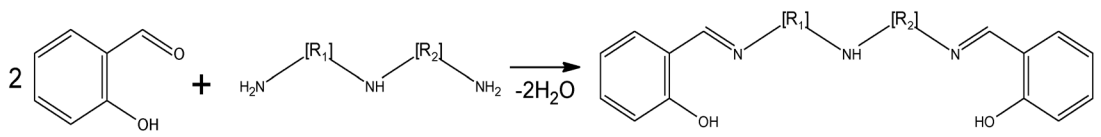

Scheme 1 Schiff condensation resulting in H_2*saldet* (R_1 = R_2 = CH_2CH_2), H_2*salpet* (R_1 = $CH_2CH_2CH_2$, R_2 = CH_2CH_2), H_2*saldpt* (R_1 = R_2 = $CH_2CH_2CH_2$), and H_2*saldptm* (R_1 = R_2 = $CH_2CH_2CH_2$, NH → NCH_3); H_2*saldpt* = N,N'-bis(1-hydroxy-2-benzyliden)-1,7-diamino-4-azaheptane.

The mononuclear precursors were prepared by the following general recipe. Methanol solution of the ligand H_2L^5 was combined with methanol solution of Fe(III) halide ($FeCl_3 \cdot 6H_2O$) accompanied by color change. Then triethyalmine was added. After stirring at 50 °C for a couple of minutes, the reacting mixture is cooled to room temperature. The precipitated crystalline powder [$Fe^{III}L^5Cl$] was separated by filtration, washed, and dried. The elemental analysis confirmed the expected C/H/N contents.

The methanol solution of [Fe(*salpet*)Cl] was combined with water solution of KCN (5 % excess). After short stirring, the color turned from red to dark blue, and a black crystalline powder of [Fe(*salpet*)CN] MeOH (**1c**) precipitated. The mononuclear precursors are water-sensitive. They are soluble in methanol, ethanol, acetonitrile, chlorophorm, and toluene.

Dinuclear complex [Fe(*salpet*){CN}Fe(*salpet*)]$(ClO_4) \cdot 2H_2O$ (**2a**) was prepared by combining acetonitrile solution of [Fe(*salpet*)CN] with methanol solution of $Ni(ClO_4)_2 \cdot 6H_2O$. The mixture was stirred for 2 h at 50 °C and then left to evaporate spontaneously for several days at room temperature when black crystals were separated by filtration.

Dinuclear complex [Fe(MeBu-*salpet*){CN}Fe(MeBu-*salpet*)][BPh_4]$\cdot 2CH_3CN$ (**2b**) was prepared by adding K[$Ag(CN)_2$] to a methanol/acetonitrile solution of [Fe(MeBu-*salpet*)Cl]. After stirring, the resulting solution was filtered to a solution of $NaBPh_4$ and left to cool down; after 3 h, green–brown crystals were separated.

Mixed-valence trinuclear complex [Fe^{III}(*salpet*){$Fe^{II}(CN)_5(NO)$}Fe^{III}(*salpet*)]$\cdot 3.65H_2O$ (**3a**) was synthesized from building blocks: methanol solution of [Fe(*salpet*)Cl] was combined with methanol/water solution of $Na_2[Fe(CN)_5(NO)] \cdot 2H_2O$. In a short time, the color turned to violet–blue. The mixture was stirred at 50 °C and then left to evaporate spontaneously for several days at room temperature when dark violet crystals were separated.

Trinuclear complex *trans*-[Fe^{III}(MeBu-*salpet*){$Ni(CN)_4$}Fe^{III}(MeBu-*salpet*)]$\cdot 2CH_3OH$ (**3b**) resulted from a combination of methanol/acetonitril solution of [Fe(MeBu-*salpet*)Cl] and $K_2[Ni(CN)_4] \cdot H_2O$. The suspension was stirred at 60 °C, the resulting solution was filtered off and left to evaporate spontaneously when black crystals were formed. In an analogous manner, the trinuclear complex [Fe^{III}(*sadptm*){$Pt(CN)_4$}Fe^{III}(*sadptmt*)] (**3c**) has been synthesized.

In preparing trinuclear complexes [Fe^{III}(MeO-*salpet*){$Ag(CN)_2$}Fe^{III}(MeO-*salpet*)]Cl (**3d**) and [Fe^{III}(EtO-*salpet*){$Ag(CN)_2$}Fe^{III}(EtO-*salpet*)]Cl (**3e**), a methanol solution of [FeL^5Cl] was combined with aqueous methanol solution of $KAg(CN)_2$. The dark black precipitate was stirred, then 60 % of the solvent was reduced using a rotary evaporator at temperatures never higher than 35 °C. Water was added in order to precipitate the complex, and on cooling the yield was enhanced.

In all cases, the elemental analysis confirmed the expected C/H/N contents in a satisfactory agreement. The complexes were characterized by IR and UV–vis spectra. IR spectra were measured in KBr pellets (Magna FTIR 750, Nicolet) in the 4000–400 cm^{-1} region. Electronic spectra were measured using the DRIFT method (Magna FTIR 750 Nicolet) in the region 5000–11 000 cm^{-1} and in Nujol mull (Specord 200, Analytical Jena) in the range 10 000–50 000 cm^{-1}.

Structural data

The structure of the mononuclear, dinuclear, and trinuclear complexes has been determined by single-crystal X-ray analysis, primarily at room temperature. The corresponding visualization ("Mercury") for seven new complexes is shown in Figs. 5–7 along with two CCDC entries. For three analogous complexes, the structure is only expected (Fig. 8) because of a lack of single crystals.

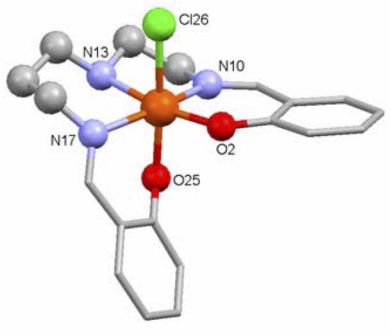

[Fe(*salpet*)Cl], (**1a**) [17]

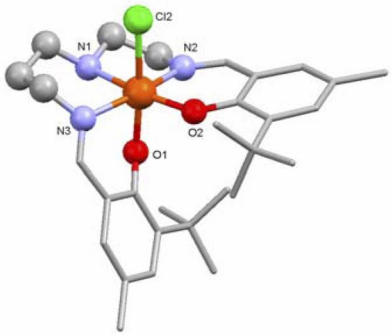

[Fe(MeBu-*saldpt*)Cl], (**1b**) [17]

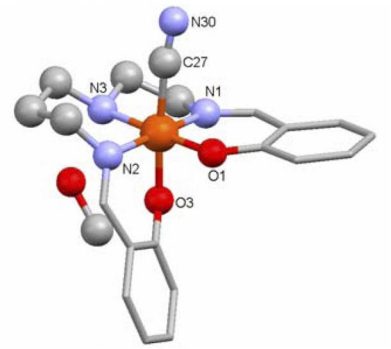

[Fe(*salpet*)(CN)]·MeOH, **1c** [17]

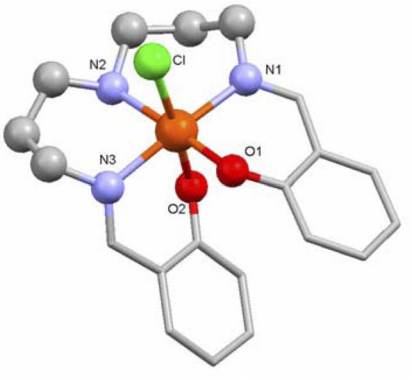

[Fe(*saldpt*)Cl], (**1d**), SIMPFE [18]

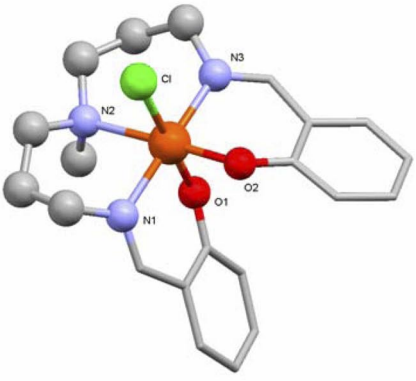

[Fe(*saldptm*)Cl], (**1e**), XOFDOL [19]

Fig. 5 Molecular structure of mononuclear precursors.

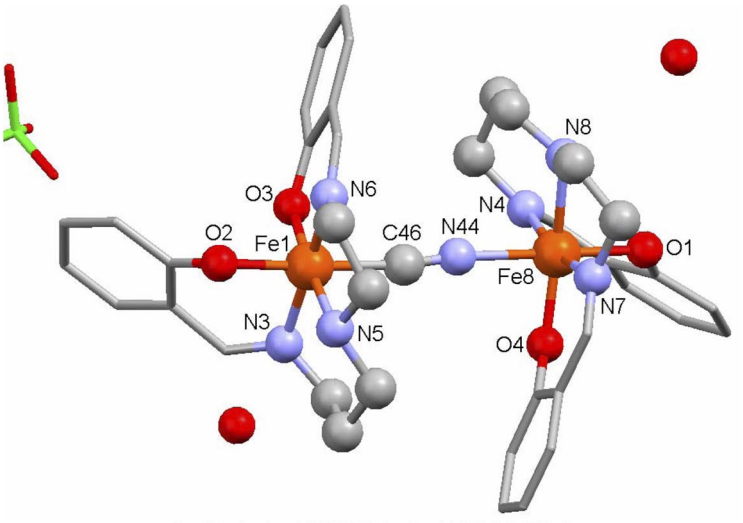

2a, [Fe(*salpet*){CN}Fe(*salpet*)](ClO$_4$)·2H$_2$O

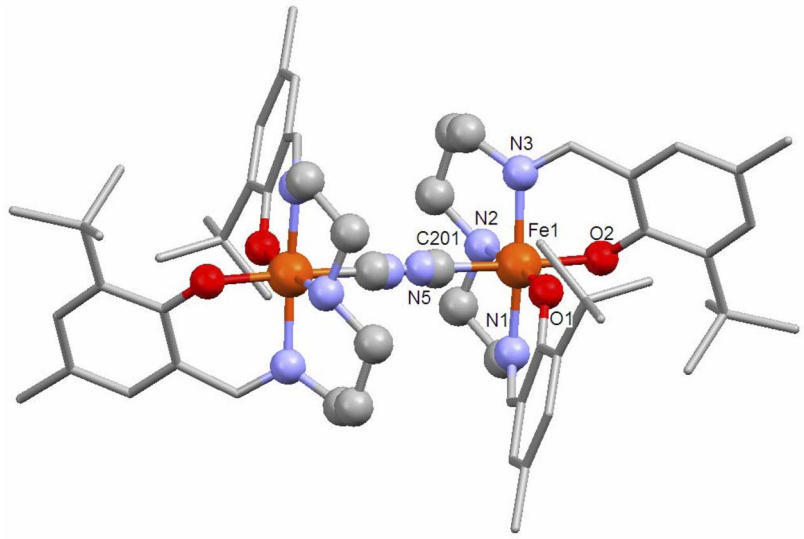

2b, [Fe(MeBu-*salpet*){CN}Fe(MeBu-*salpet*)][BPh$_4$].2CH$_3$CN, 90 K

Fig. 6 Molecular structure of cyano-bridged dinuclear complexes [17]. The CN bridge in **2b** is disordered.

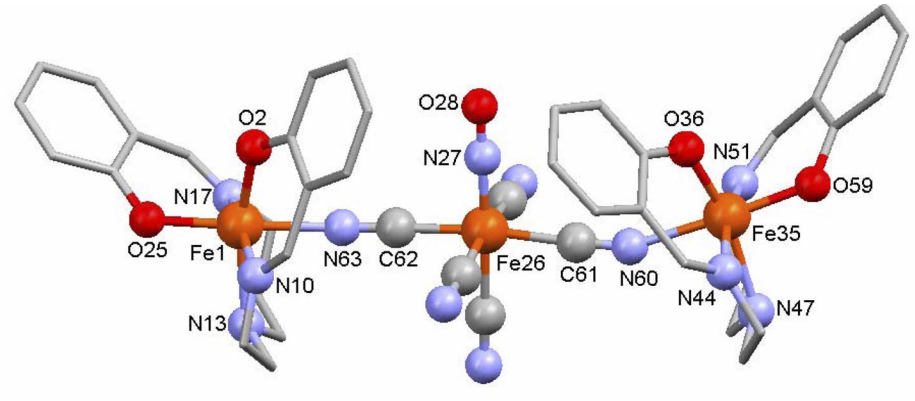

3a, $[Fe^{III}(salpet)\{Fe^{II}(CN)_5(NO)\}Fe^{III}(salpet)]\cdot 3.65H_2O$

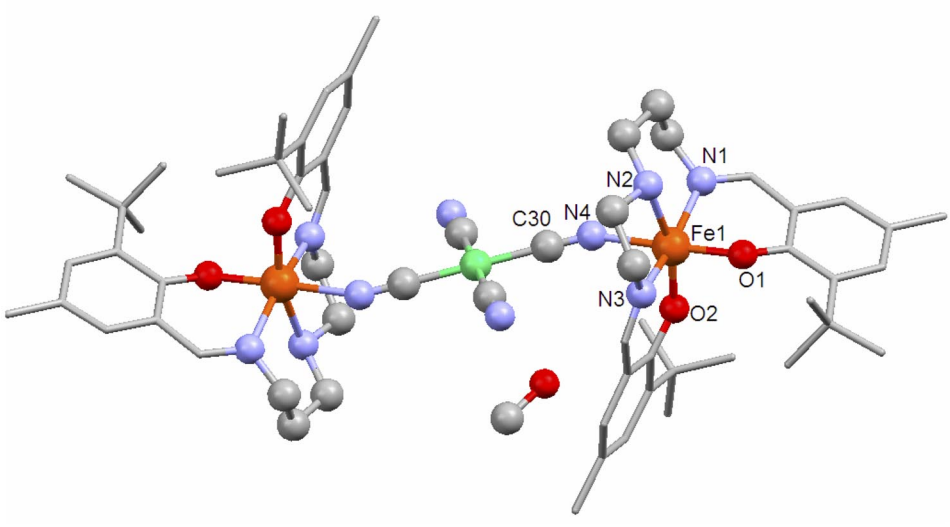

3b, $[Fe^{III}(MeBu\text{-}salpet)\{Ni(CN)_4\}Fe^{III}(MeBu\text{-}salpet)]\cdot 2CH_3OH$

Fig. 7 Molecular structure of metallacyano-bridged trinuclear complexes [17].

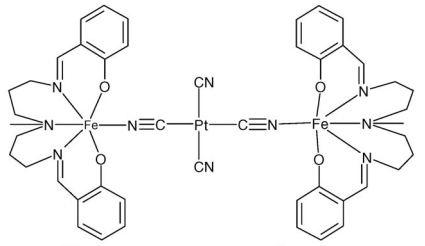

3c, [Fe^{III}(*saldptm*){$Pt(CN)_4$}Fe^{III}(*saldptm*)]

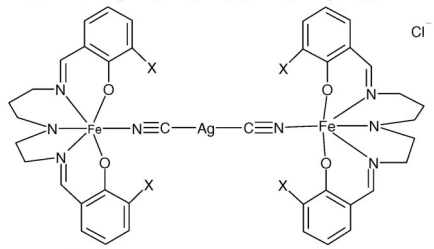

3d, [Fe^{III}(MeO-*salpet*){$Ag(CN)_2$}Fe^{III}(MeO-*salpet*)]Cl
3e, [Fe^{III}(EtO-*salpet*){$Ag(CN)_2$}Fe^{III}(EtO-*salpet*)]Cl

Fig. 8 Expected molecular structure of trinuclear complexes.

The metal–ligand distances inside the chromophores are listed in Table 1. These serve as a sensitive indicator of the spin state of the complex. The averaged metal–ligand distances in the mononuclear cyano-containing complex **1c** are significantly shorter (Fe–O = 1.88, Fe–N = 1.95 Å) when compared to the chloro-containing analogs **1a** (Fe–O = 1.94, Fe–N = 2.15 Å) and **1b** (Fe–O = 1.93, Fe–N = 2.13 Å). This proves that **1c** is LS, whereas other mononuclear precursors are HS.

Table 1 Overview of important bond lengths.[a]

LS center		HS center	
1c, [Fe(*salpet*)CN], L{*S* = 1/2}		**1a**, [Fe(*salpet*)Cl], H{*S* = 5/2}	
Fe–O: 1.874, 1.888	av = 1.881	Fe–O: 1.916, 1.970	av = 1.943
Fe–N: 1.903, 1.940, *1.996*	av = 1.946	Fe–N: 2.100, 2.120, *2.220*	av = 2.147
		1b, [Fe(MeBu-*salpet*)Cl], H{*S* = 5/2}	
		Fe–O: 1.969, 1.897,	av = 1.933
		Fe–N: 2.093, 2.093, *2.202*	av = 2.129
		[Fe(*saldpt*)Cl], SIMPFE	
		Fe–O: 1.935, 1.975	av = 1.955
		Fe–N: 2.113, 2.102, *2.252*	av = 2.156
		[Fe(*saldptm*)Cl], XOFDOL	
		Fe–O, 1.963, 1.936	av = 1.949
		Fe–N, 2.099, 2.100, *2.313*	av = 2.141
2a, [L^5Fe{CN}FeL^5]ClO_4·$2H_2O$, L^5 = *salpet*, LH{1/2,5/2}			
Fe1–O: 1.918, 1.874;	av = 1.896	Fe8–O: 1.938, 1.900;	av = 1.919
Fe1–N: 1.928, 1.986, *2.035*	av = 1.983	Fe8–N: 2.046, 2.047, *2.138*, 2.132(NC)	av = 2.091

(*continues on next page*)

Table 1 (*Continued*).

LS center		HS center	
2b, $[L^5Fe\{CN\}_dFeL^5][BPh_4]\cdot 2CH_3CN$, L^5 = MeBu-*salpet*, T = 90 K			
Fe–O: 1.896, 1.889	av = 1.892		
Fe–N: 1.966, 1.991, *2.076*	av = 2.052		
Fe–C: 1.868 (disordered)			
Fe–N: 2.177 (disordered)			
3a, $[L^5Fe\{Fe(CN)_5NO\}FeL^5]\cdot 3.65H_2O$, L^5 = *salpet*, HH{5/2,5/2}			
		Fe1–O: 1.918, 1.937	av = 1.927
		Fe1–N: 2.101, 2.181, 2.067, 2.146(NC)	av = 2.124
		Fe35–O: 1.911, 1.933	av = 1.922
		Fe35–N: 2.095, 2.194, 2.099, 2.180(NC)	av = 2.142
3b, $[L^5Fe\{Ni(CN)_4\}FeL^5]\cdot 2CH_3OH$, L^5 = MeBu-*salpet*, HH{5/2,5/2}			
		Fe–O: 1.901, 1.917	av = 1.909
		Fe–N: 2.083, 2.098, 2.239, 2.158(NC)	av = 2.145

[a]The longest Fe–N distance corresponding to the tertiary amine is given in italics.

In the molecular structure of the dinuclear complex **2a**, the *mer*-$\{FeN_3O_2X\}$ configuration of the chromophore found for mononuclear precursor is maintained (Fig. 6). The C-donor atom of the cyanide group coordinates to the first Fe(III) center and the corresponding contact (Fe1–C = 1.996 Å) is a bit longer relative to the mononuclear precursor **1c** (1.961 Å). The CN group exhibits the bond length typical for a triple bond (1.144 Å), and it is coordinated in nearly linear manner. Its N-donor atom possesses much longer contact to the second central atom (N–Fe8 = 2.132 Å). The contacts Fe1–N(av) = 1.983 Å are generally shorter than Fe8–N(av) = 2.091 Å; this could indicate that the first Fe(III) center is LS whereas the second Fe(III) center is HS at room temperature. The distances to the apical oxygen atoms are Fe1–O2 = 1.918 and Fe8–O1 = 1.938 Å, as compared to the mononuclear ones: Fe–O25 = 1.970, Fe–O1 = 1.969; Fe–O3 = 1.888 Å for **1a**, **1b**, and **1c**, respectively; they span the interval in-between the pure LS and HS states.

The molecular structure (90 K) for the second dinuclear complex **2b** is displayed in Fig. 6. The cyanide group is disordered owing to the presence of the inversion center just in-between the Fe atoms. The bridge is almost linear. The Fe1–O2 distance is short (1.889 Å) showing predominantly an LS character of the Fe centers. The Fe–C and Fe–N bond lengths to the cyanide ligand are 1.868 and 2.177 Å, respectively. The averaged distances Fe–O(av) = 1.892 and Fe–N(av) = 2.052 Å at T = 90 K lie in-between the pure LS and HS range.

The molecular structure of the trinuclear complex **3a** is viewed in Fig. 7. The peripheral Fe(III) centers are Fe–NC-coordinated at the distances characteristic for HS complexes (Fe1–N = 2.146, Fe35–N = 2.180 Å); the other Fe–N(amine) contacts are also rather long (2.101, 2.181, 2.067, 2.095, 2.194, 2.099 Å). The N–C bond lengths adopt characteristic values (1.155 and 1.127 Å) and are a bit bent-coordinated (Fe1–N–C = 161, Fe35–N–C = 158 deg). The nitrosyl group is linearly coordinated to the very central Fe(II) atom at a short contact (Fe–N = 1.657, N–O = 1.131 Å).

The molecular structure of the trinuclear complex **3b** is shown in Fig. 7. The complex is centrosymmetric, and according to the metal–ligand distances it is HS at room temperature: Fe–O(av) = 1.909, and Fe–N(av) = 2.145 Å.

MÖSSBAUER SPECTRA

A conventional spectrometer has been used in scanning the MS at liquid-helium and room temperature (^{57}Co/Rh source, calibration at α-Fe at room temperature).

The presence of the Fe(III) center in mononuclear complexes manifests itself in MS by a quadrupole doublet with the characteristic quadrupole splitting $Q \sim 0.7$ and isomer shift $\delta \sim 0.3$ (all data in mm s^{-1}), which are temperature-independent as listed in Table 2.

Table 2 Mössbauer-spectra parameters.

T/K	Center	Quadrupole splitting, *Q*/mm s^{-1}	Isomer shift, δ/mm s^{-1}	Area/%[a]
1a, [Fe(*salpet*)Cl]				
20	HS-Fe(III)	0.676	0.376	100
300	HS-Fe(III)	0.648	0.254	100
2a, [Fe(*salpet*){CN}Fe(*salpet*)](ClO_4)·2H_2O				
20	LS-Fe(III)	2.56	0.047	62
	HS-Fe(III)	0.96	0.308	38
300	LS-Fe(III)	2.36	–0.028	39
	HS-Fe(III)	0.90	0.239	61
3a, [Fe^{III}(*salpet*){$Fe^{II}(CN)_5(NO)$}Fe^{III}(*salpet*)]·3.65H_2O				
20	LS-Fe(III)	2.706	0.073	46
	HS-Fe(III)	0.851	0.323	38 (45.0)
	LS-Fe(II)	1.951	–0.319	16
78	LS-Fe(III)	2.681	0.071	44
	HS-Fe(III)	0.854	0.319	38 (46.1)
	LS-Fe(II)	1.905	–0.334	18
200	LS-Fe(III)	2.641	0.030	41
	HS-Fe(III)	0.872	0.294	43 (51.1)
	LS-Fe(II)	1.857	–0.354	16
295	LS-Fe(III)	2.443	–0.032	23
	HS-Fe(III)	0.913	0.218	59 (72.4)
	LS-Fe(II)	1.802	–0.379	18
300	LS-Fe(III)	2.463	–0.044	22
	HS-Fe(III)	0.800	0.222	65 (74.9)
	LS-Fe(II)	1.800	–0.346	13
3d, [Fe^{III}(MeO-*salpet*){$Ag(CN)_2$}Fe^{III}(MeO-*salpet*)]Cl				
20	LS-Fe(III)	2.60	0.10	10
	HS-Fe(III)	0.79	0.37	90
3e, [Fe^{III}(EtO-*salpet*){$Ag(CN)_2$}Fe^{III}(EtO-*salpet*)]Cl				
20	LS-Fe(III)	2.63	0.08	17
	HS-Fe(III)	0.80	0.37	83

[a]Values in parentheses refer to the renormalized HS mole fraction.

For the dinuclear complex **2a**, the MS characteristics for the LS centers ($Q = 2.56, 2.36$; $\delta = 0.047$, –0.028) and the HS centers ($Q = 0.96, 0.90$; $\delta = 0.308, 0.293$) change little between $T = 20$ and 300 K, respectively. However, the corresponding area fraction (A) rises in favor of the HS state (from 38 to 61 % of the HS fraction), Fig. 9. This excludes constant amounts 50 % of LS and 50 % of HS, and unambiguously shows that the complex exhibits a kind of the spin crossover.

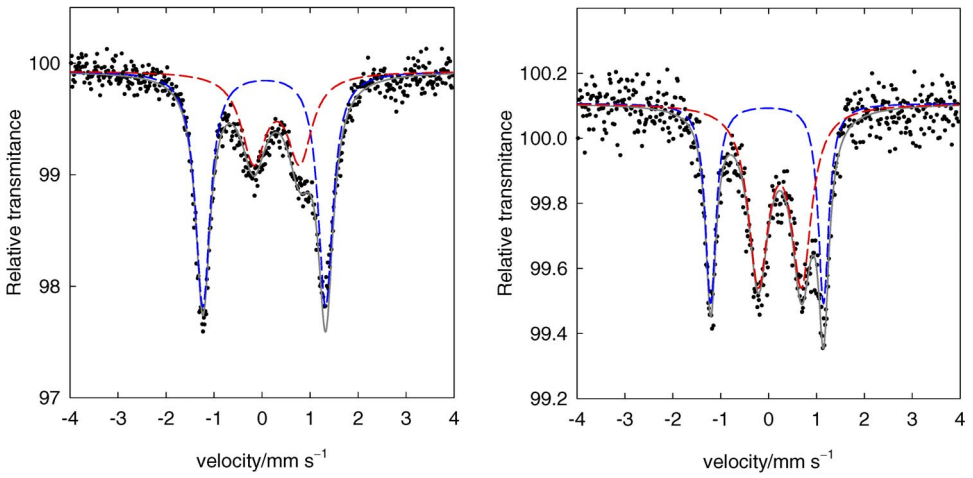

Fig. 9 MS of the dinuclear complex **2a** at T = 20 K (left) and T = 300 K (right). Dashed lines: deconvolution to the LS and HS quadrupole doublets.

The MS for the complex **3a** (Fig. 10) show a coexistence of the LS and HS Fe(III) centers even at temperature as low as T = 20 K. The spectra are complex since the Fe(III) centers are not perfectly equivalent. Deconvolution to three quadrupole doublets shows that on warming, a spin crossover proceeds: the Fe(III) center passes from the LS state to the HS one. The HS mole fraction for Fe(III) centers has been renormalized due to the presence of the spin-crossover silent Fe(II) centers.

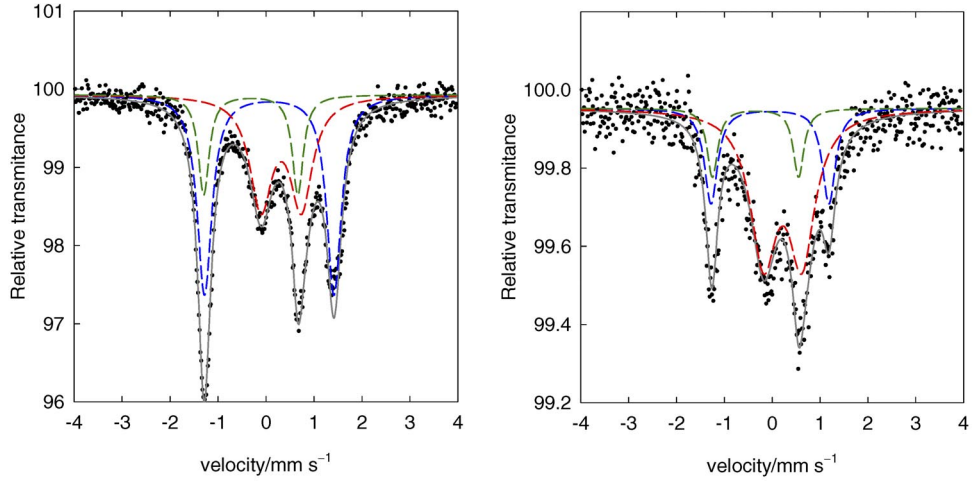

Fig. 10 MS of the trinuclear complex **3a** at T = 20 K (left) and T = 300 K (right). Dashed lines: deconvolution to three quadrupole doublets.

The MS for a pair of complexes with the $\{Ag(CN)_2\}$ bridge, **3d** and **3e**, show a dominant HS portion of Fe(III) with some "residual" LS phase at T = 20 K (Fig. 11).

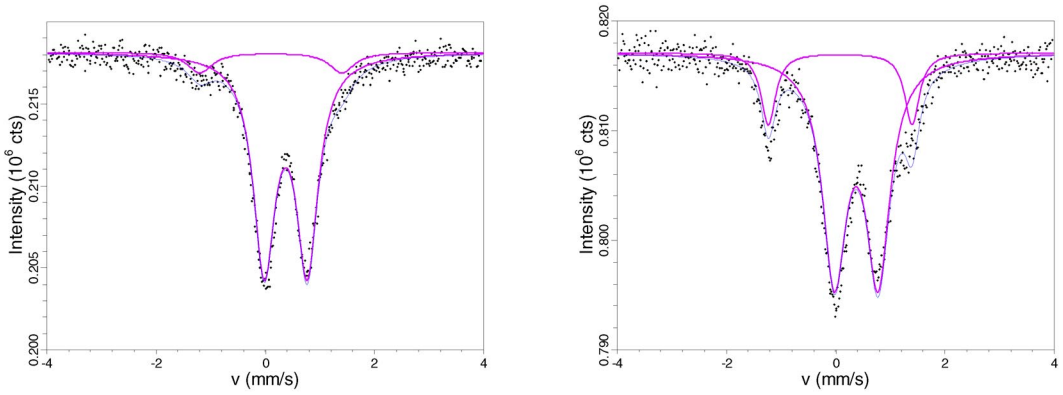

Fig. 11 MS of the trinuclear complex **3d** (left) and **3e** (right) at T = 20 K. Minor lines: deconvolution into two quadrupole doublets.

MAGNETIC DATA

Magnetic susceptibility and magnetization measurements were done using a SQUID magnetometer (Quantum Design) from 2 K at B = 0.1 T. The magnetization data were taken at T = 2.0 and 4.6 K, respectively. Raw susceptibility data were corrected for underlying diamagnetism using the set of Pascal constants. The effective magnetic moment has been calculated as usual: $\mu_{\text{eff}}/\mu_{\text{B}} = 798(\chi' T)^{1/2}$ when SI units are employed.

The magnetic data for complexes which preserve their spin state over the whole temperature range can be processed by the standard apparatus of the molecular magnetism [2,3,20]. In fact, the spin-Hamiltonian formalism has been applied. For mononuclear complexes, it accounts for the zero-field splitting, Zeeman term, and eventual molecular-field correction

$$\hat{H} = \hbar^{-2}[D(\hat{S}_z^2 - \hat{S}^2/3) + E(\hat{S}_x^2 - \hat{S}_y^2)] + \hbar^{-1} g\mu_{\text{B}} B\hat{S}_a - \hbar^{-1}(zj)\left\langle S_z \right\rangle \hat{S}_z \tag{1}$$

(a = x, y, z). For magnetic diads, it accounts for the isotropic exchange, asymmetric exchange, and Zeeman term

$$\begin{aligned}\hat{H} = &-J(\vec{S}_A \cdot \vec{S}_B)\hbar^{-2} + (\vec{S}_A \cdot \bar{\bar{D}}_A \cdot \vec{S}_A + \vec{S}_B \cdot \bar{\bar{D}}_B \cdot \vec{S}_B)\hbar^{-2} + (\vec{S}_A \cdot \bar{\bar{D}}_{AB} \cdot \vec{S}_B)\hbar^{-2} \\ &+\hbar^{-1}\mu_{\text{B}}(g_A \vec{B} \cdot \vec{S}_A + g_B \vec{B} \cdot \vec{S}_B)\end{aligned} \tag{2}$$

The functional to be minimized, $(\partial F/\partial p_i) = 0$, consists of two weighted datasets: the magnetic susceptibility and the molar magnetization, either

$$F(...p_i...) = \left[w_1 (1/n) \sum_n^N \left| \frac{\chi_n^{\text{o}} - \chi_n^{\text{c}}}{\chi_n^{\text{o}}} \right| \right] + \left[w_2 (1/m) \sum_m^M \left| \frac{M_m^{\text{o}} - M_m^{\text{c}}}{M_m^{\text{o}}} \right| \right] \tag{3a}$$

or

$$F(...p_i...) = \left[(1/n) \sum_n^N \left| \frac{\chi_n^{\text{o}} - \chi_n^{\text{c}}}{\chi_n^{\text{o}}} \right| \right] \times \left[(1/m) \sum_m^M \left| \frac{M_m^{\text{o}} - M_m^{\text{c}}}{M_m^{\text{o}}} \right| \right] \tag{3b}$$

The above-postulated functional accounts for all data points uniformly, through their relative errors. The calculated magnetic parameters are listed in Table 3.

Table 3 Calculated spin-Hamiltonian parameters.

Parameter	**1c**	**1a**	**3b**	**3c**
g_L	2.36			
g_H		1.813	2.010	2.013
$(D_H/hc)/cm^{-1}$		1.52	0.45	–0.89
$(E_H/hc)/cm^{-1}$		0.33		
$(zj/hc)/cm^{-1}$	–0.17			
$\chi_{TIP}/(10^{-9}\ m^3\ mol^{-1})$	0.76	4.99		
$(J_{HH}/hc)/cm^{-1}$			+0.085	–0.192
$R(\chi)$	0.019	0.010	0.019	0.010
$R(M)$			0.013	0.033

The mononuclear precursor [Fe^{III}(*salpet*)Cl], **1a**, is HS. Its effective magnetic moment at room temperature is μ_{eff} = 5.7 μ_B, and it slowly decreases on cooling (Fig. 12). This reflects the Curie law fulfilled at higher temperature with some temperature-independent paramagnetism (TIP). On cooling

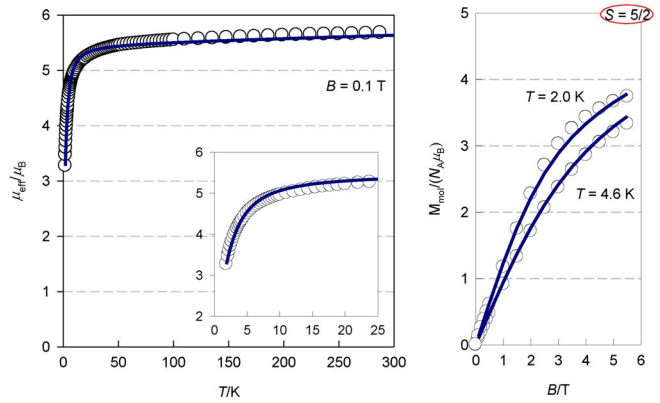

1a, [Fe(*salpet*)Cl], high-spin

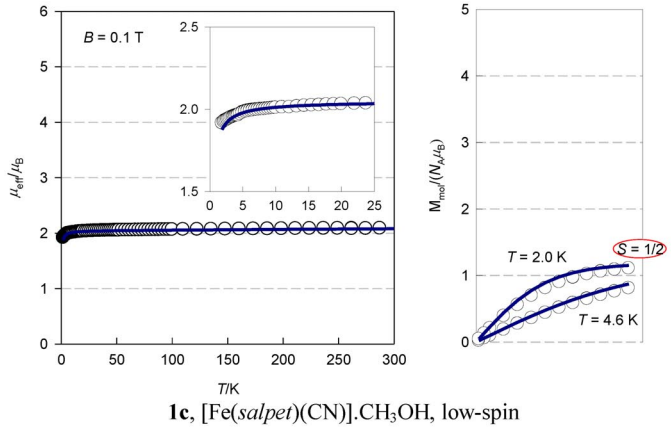

1c, [Fe(*salpet*)(CN)].CH_3OH, low-spin

Fig. 12 Magnetic data for mononuclear Fe(III) complexes **1a** and **1c**. Left: temperature dependence of the effective magnetic moment; right: field dependence of the magnetization. Solid lines: fitted data.

below 25 K, the μ_{eff} drops down and adopts a value of μ_{eff} = 3.3 at T = 1.8 K. The calculated spin-Hamiltonian parameters for S = 5/2 are: g = 1.813, D/hc = 1.52 cm^{-1}, E/hc = 0.33 cm^{-1}, and χ_{TIP} = 4.99×10^{-9} m^3 mol^{-1}. The lowered g-factor relative to the spin-only value originates in an orbital contribution within the {FeN_3O_2Cl} chromophore.

The mononuclear complex [Fe^{III}(*salpet*)(CN)]·CH_3OH, **1c**, is LS owing to the high CF strength of the cyano-ligand (Fig. 12). For S = 1/2 paramagnet the Curie law provides temperature development of μ_{eff} along a straight line; the model can be improved by the TIP correction, as well as by the molecular field correction effective at low temperature. The magnetic parameters g = 2.36, $\chi_{TIP} = 0.76 \times 10^{-9}$ m^3 mol^{-1}, and zj/hc = –0.17 cm^{-1} reproduce the susceptibility satisfactorily; however, the magnetization data are not reproduced as well. The g-value indicates an orbital contribution within the {FeN_3O_2C} chromophore relative to the spin-only value. In a hypothetical octahedral geometry, the reference CF term $^2T_{2g}$ is orbitally degenerate and the Griffith–Figgis model of symmetry lowering would be more appropriate than the simple Curie law [2,3,20].

Two trinuclear complexes, **3b** and **3c**, possessing magnetic diads [the very central units {$Ni^{II}(CN)_4$} and {$Pt^{II}(CN)_4$} are diamagnetic] show a saturation of magnetization $M_{mol}/N_A \sim 10\ \mu_B$ at 2 K; they exhibit an analogous high-temperature tail of the effective magnetic moment $\mu_{eff} \sim 8.4\ \mu_B$ (Fig. 13). On cooling, the effective magnetic moment for **3b** slightly increases, indicating that the exchange coupling of the ferromagnetic nature, $J_{HH} > 0$, applies and the ground state is S = 5. The magnetic data can be fitted with only two parameters: g_H = 2.010, J_{HH}/hc = +0.069 cm^{-1}. With such a small exchange coupling constant the band, formed of N = 36 magnetic energy levels between S_{max} = 10 and S_{min} = 0, is very narrow, since

$$\Delta\varepsilon = JS_{min}(S_{min}+1)/2 - JS_{max}(S_{max}+1)/2 = -15J \approx 1\ \text{cm}^{-1} \tag{4}$$

The 11-member S = 5 manifold $|S,M_S\rangle$ can be further split by the single-ion anisotropy term. Its involvement improves the low-temperature, high-field magnetization data: g_H = 2.010, J_{HH}/hc = +0.085 cm^{-1}, D_H/hc = 0.45 cm^{-1}. However, the functional is little sensitive to the sign and magnitude of D_H (a reliable bracketing of D_H requires experimental data taken at much lower temperature). On the contrary, the effective magnetic moment for **3c** on cooling decreases so that $J_{HH} < 0$ applies in this case and then we got: g_H = 2.013, J_{HH}/hc = –0.192 cm^{-1}, D_H/hc = –0.89 cm^{-1}. Again, the involvement of the single-ion anisotropy term improves the low-temperature, high-field magnetization data, although the functional is little sensitive to the sign and magnitude of D_H. The switch of the ferromagnetic coupling to the antiferromagnetic one can be caused by a more diffuse character of the Pt(5d) orbitals, giving rise to a more effective kinetic super-exchange.

Five complexes consisting of magnetic diads (**2a**, **2b**, **3a**, **3d**, and **3e**) show a kind of spin crossover, and analysis of their magnetic and Mössbauer data requires a novel theoretical model.

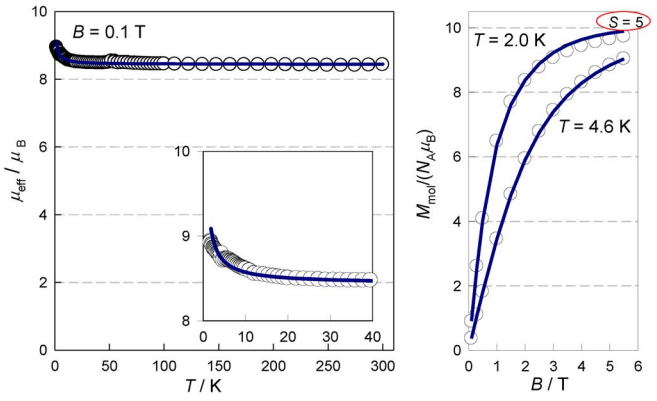

3b, [(MeBu-*salpet*)Fe^{III}{$Ni^{II}(CN)_4$}Fe^{III}(MeBu-*salpet*)]·$2CH_3OH$,
high-spin, ferromagnetic exchange

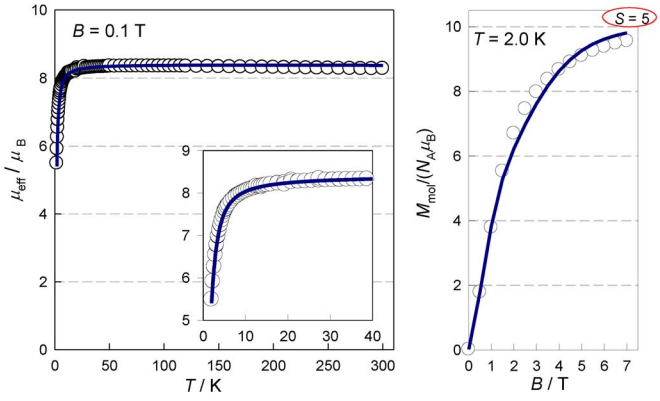

3c, [(*saldptm*)Fe^{III}{$Pt^{II}(CN)_4$}Fe^{III}(*saldptm*)],
high-spin, antiferromagnetic exchange

Fig. 13 Magnetic data for trinuclear complexes **3b** and **3c** with exchange interaction between two Fe(III) centers. Solid lines: fitted data. Classification: A/HH group.

THEORETICAL

The existing spin-crossover models proposed for the dinuclear systems are heavily oversimplified [21,22]. Their application to the present data was unsuccessful. Therefore, there is a need for outlining a more general and more flexible model that could be applied in the data fitting. The requirement is to recover the susceptibility, low-temperature magnetization, and Mössbauer data by the same set of free parameters.

The theoretical model outlined here refers to the situation depicted in Fig. 14. Under the reference state, it is assumed the situation with defined spin at each site. As it could be either low-spin (L) or high-spin (H), we meet four reference states.

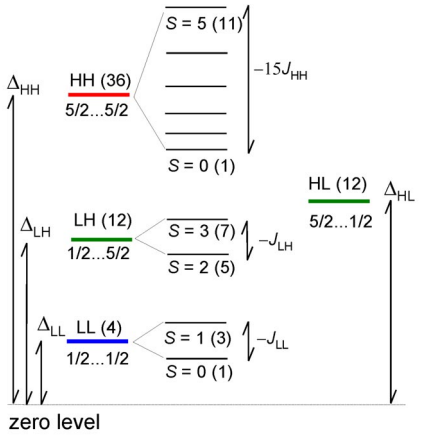

Fig. 14 Reference states (LL, LH, HL, HH) and the corresponding spin multiplets (multiplicities in parentheses) for a dinuclear Fe(III) system.

1. Four reference electronic states, i.e., LL, LH, HL, and HH, can be characterized by a common spin Hamiltonian involving the isotropic exchange coupling and the spin-Zeeman term

$$\hat{H}_{ab}^{\text{spin}} = -J_{ab}(\vec{S}_a \cdot \vec{S}_b)\hbar^{-2} + \mu_B B(g_a \vec{S}_a + g_b \vec{S}_b)\hbar^{-1} \tag{5}$$

   where the (*ab*) set is either LL, LH, HL, or HH pair. For the LL pair, there are 4 energy levels $\varepsilon_{LL}(S, M_S)$ with $S \in <0, 1>$, for the LH (HL) pair there are 12 energy levels $\varepsilon_{LH}(S, M_S)$ with $S \in <2, 3>$, and for the HH pair there are 36 energy levels $\varepsilon_{HH}(S, M_S)$ with $S \in <0, 5>$.
2. Except for two specific cases (the LL and HH reference states with the equivalent *g*-factors), the spin Hamiltonian does not adopt a diagonal form. The exact treatment needs a diagonalization of the spin-Hamiltonian matrix for a defined magnetic field. For such a purpose, three magnetic fields are selected near the reference, say, $B_{r,k} = B_r$, $B_r + \delta$, and $B_r + 2\delta$, where δ is a small increment ($\delta = B_r/100$). The eigenvalue routine returns three sets of energy levels $\varepsilon_i(S,M_S; B_{r,k})$. They can be fitted by a parabola so that the van Vleck coefficients in the form $\varepsilon_i(B_r) = \varepsilon_i^{(0)} + \varepsilon_i^{(1)} B_r + \varepsilon_i^{(2)} B_r^2$ can be numerically identified.
3. The total electronic partition function of the system is constructed as follows

$$\begin{aligned} Z(B_r,T) &= \sum_{j=1}^{64} \exp[-E_j(B_r)/kT] \\ &= \sum_{i=1}^{4} \exp[-(\Delta_{LL} + \varepsilon_{LL_{i,r}})/kT] + \sum_{i=1}^{12} \exp[-(\Delta_{LH} + \varepsilon_{LH_{i,r}})/kT] \\ &+ \sum_{i=1}^{12} \exp[-(\Delta_{HL} + \varepsilon_{HL_{i,r}})/kT] + \sum_{i=1}^{36} \exp[-(\Delta_{HH} + \varepsilon_{HH_{i,r}})/kT] \end{aligned} \tag{6}$$

   Here, the energy separations, Δ_{LL}, Δ_{LH}, Δ_{HL}, and Δ_{HH}, need to be considered as external parameters since they do not enter the spin Hamiltonian. They originate in the orbital angular momentum and relate to the actual CF strength in the complex under study. (One of them needs to be fixed, say, $\Delta_{LL} = 0$.) Normally, $\Delta_{LH} = \Delta_{HL}$ is assumed for symmetric centers; however, this is not generally fulfilled.
4. The molar magnetization is defined through the first derivative of the partition function at the reference field B_r

$$M_{\mathrm{mol}}(B_r,T) = N_{\mathrm{A}}kT\left(\frac{\partial \ln Z}{\partial B}\right)_{B_r} = N_{\mathrm{A}}kT(c_T^{(1)} + 2c_T^{(2)}\boldsymbol{B}_r) \tag{7}$$

where the logarithm of the partition function has been fitted by a parabola

$$\ln Z(B_r,T) = c_T^{(0)} + c_T^{(1)}B_r + c_T^{(2)}B_r^2 \tag{8}$$

Alternatively, with the use of the van Vleck coefficients it becomes expressed as

$$M_{\mathrm{mol}}(B_r,T) = N_{\mathrm{A}}\left(\frac{\partial \ln Z}{\partial B}\right)_{B_r} = N_{\mathrm{A}}\frac{\sum_{j=1}^{64} -(\varepsilon_j^{(1)} + 2\varepsilon_j^{(2)}B_r)\exp[-\varepsilon_j(B_r)/kT]}{Z(B_r)} \tag{9}$$

5. At a low magnetic field (B_0 = 0.1 T), we are left with a linear magnetic material and thus

$$\chi_{\mathrm{mol}}(B_0,T) = \mu_0\left(\frac{\partial M_{\mathrm{mol}}(B)}{\partial B}\right)_{B_0} = \mu_0 N_{\mathrm{A}}kT(2c_T^{(2)}) \tag{10}$$

Alternatively, the van Vleck formula for the magnetic susceptibility is applicable

$$\bar{\chi}_{\mathrm{mol}}(B_0,T) = N_{\mathrm{A}}\mu_0\frac{\sum_{j=1}^{64}\{[\varepsilon_j^{(1)}]^2/kT - 2\varepsilon_j^{(2)}\}\exp(-\varepsilon_j^{(0)}/k\boldsymbol{T})}{\sum_{j=1}^{64}\exp(-\varepsilon_j^{(0)}/kT)} \tag{11}$$

where the van Vleck coefficients refer to the small reference field B_0.

6. The case of the non-isotropic, asymmetric exchange can be put into operation by enlarging the spin Hamiltonian for the corresponding interactions and then performing its diagonalization for individual reference states (LL, LH, HL, and HH). The coupling, in fact, is only a unitary transformation that leaves the eigenvalues invariant. Therefore, the coupling process could be omitted completely (as a redundant and tedious operation) and the matrix elements can be generated in the basis set of uncoupled spin functions [20].

The outlined theory could work properly on two assumptions: (i) there is not a substantial solid-state cooperativeness (an extra interaction energy preferring the spin-like pairs); (ii) there is not a substantial contribution from molecular vibrations to the partition function.

The solid-state cooperativeness could be accounted for by modifying the spin-crossover model for dinuclear systems outlined by Bousseksou [22]. The key modification is a removal of the constraint that there is single site-formation parameter (Δ_0); instead, we have to deal with (Δ_{LL}), Δ_{LH}, Δ_{HL}, and Δ_{HH} reference energies.

The second aspect requires a redefinition of the partition function, which includes the summations over spin multiplets for individual reference electronic states, each multiplied by an appropriate vibrational partition function

$$\begin{aligned} Z = {} & z_{\mathrm{LL}}\cdot\sum_{i=1}^{4}\exp[-(\Delta_{\mathrm{LL}} + \varepsilon_{\mathrm{LL}_i})/kT] + z_{\mathrm{LH}}\cdot\sum_{i=1}^{12}\exp[-(\Delta_{\mathrm{LH}} + \varepsilon_{\mathrm{LH}_i})/kT] \\ & + z_{\mathrm{HL}}\cdot\sum_{i=1}^{12}\exp[-(\Delta_{\mathrm{HL}} + \varepsilon_{\mathrm{HL}_i})/kT] + z_{\mathrm{HH}}\cdot\sum_{i=1}^{36}\exp[-(\Delta_{\mathrm{HH}} + \varepsilon_{\mathrm{HH}_i})/kT] \end{aligned} \tag{12}$$

This enables the writing of the Boltzmann population factors

$$P_{ab} = \{z_{ab} \cdot \sum_{i=1} \exp[-(\Delta_{ab} + \varepsilon_{ab_i})/kT]\}/Z \tag{13}$$

that obey the normalization

$$1 = P_{\mathrm{LL}} + P_{\mathrm{LH}} + P_{\mathrm{HL}} + P_{\mathrm{HH}} \tag{14}$$

The HS mole fraction is calculated as

$$x_{\mathrm{HS}} = (0 \cdot P_{\mathrm{LL}} + 1 \cdot P_{\mathrm{LH}} + 1 \cdot P_{\mathrm{HL}} + 2 \cdot P_{\mathrm{HH}})/2 \tag{15}$$

and this quantity is comparable to the area fraction detected in MS.

The vibrational partition functions are considered in a more explicit form, by considering $m = 3n - 6$ vibrational modes. For a single chromofore, it is [20]

$$z_a = \exp[-\sum_{m=1}^{3n-6} (h\nu_{a,m}/2kT)] \prod_{m=1}^{3n-6} \frac{1}{1-\exp(-h\nu_{a,m}/kT)} \tag{16}$$

with a = L or H; $m = 15$ for a hexacoordinated metal center ($n = 7$). It is assumed that the vibrations of individual centers are independent, and thus the vibration partition function for a pair of centers is a product $z_{ab} = z_a \cdot z_b$. To a further approximation, the average vibration frequencies $\bar{\nu}_{\mathrm{H}}$ and $\bar{\nu}_{\mathrm{L}}$ are introduced (Einstein modes), hence

$$z_a = \frac{\exp[-(mh\bar{\nu}_a/2)/kT]}{[1-\exp(-h\bar{\nu}_a/kT)]^m} \tag{17}$$

(In order to reduce the number of free parameters, $h\bar{\nu}_{\mathrm{L}} = 1.5(h\bar{\nu}_{\mathrm{H}})$ can be accepted [23,24].) With these definitions, the total partition function can be rewritten to the final form

$$\begin{aligned} Z = {} & \left\{\frac{\exp[-(mh\bar{\nu}_{\mathrm{L}}/2)/kT]}{[1-\exp(-h\bar{\nu}_{\mathrm{L}}/kT)]^m}\right\}^2 \sum_{i=1}^{4} \exp[-(\Delta_{\mathrm{LL}} + \varepsilon_{\mathrm{LL}_i})/kT] \\ & + \left\{\frac{\exp[-(mh\bar{\nu}_{\mathrm{L}}/2)/kT]}{[1-\exp(-h\bar{\nu}_{\mathrm{L}}/kT)]^m}\right\}\left\{\frac{\exp[-(mh\bar{\nu}_{\mathrm{H}}/2)/kT]}{[1-\exp(-h\bar{\nu}_{\mathrm{H}}/kT)]^m}\right\} \sum_{i=1}^{12} \exp[-(\Delta_{\mathrm{LH}} + \varepsilon_{\mathrm{LH}_i})/kT] \\ & + \left\{\frac{\exp[-(mh\bar{\nu}_{\mathrm{L}}/2)/kT]}{[1-\exp(-h\bar{\nu}_{\mathrm{L}}/kT)]^m}\right\}\left\{\frac{\exp[-(mh\bar{\nu}_{\mathrm{H}}/2)/kT]}{[1-\exp(-h\bar{\nu}_{\mathrm{H}}/kT)]^m}\right\} \sum_{i=1}^{12} \exp[-(\Delta_{\mathrm{HL}} + \varepsilon_{\mathrm{HL}_i})/kT) \\ & + \left\{\frac{\exp[-(mh\bar{\nu}_{\mathrm{H}}/2)/kT]}{[1-\exp(-h\bar{\nu}_{\mathrm{H}}/kT)]^m}\right\}^2 \sum_{i=1}^{36} \exp[-(\Delta_{\mathrm{HH}} + \varepsilon_{\mathrm{HH}_i})/kT] \end{aligned} \tag{18}$$

Its more transparent image reads

$$\begin{aligned} Z = {} & z_{\mathrm{L}}^2 \{\sum_{i=1}^{4} \exp[-(\Delta_{\mathrm{LL}} + \varepsilon_{\mathrm{LL}_i})/kT] + r_{\mathrm{L}}^{\mathrm{H}} \sum_{i=1}^{12} \exp[-(\Delta^*_{\mathrm{LH}} + \varepsilon_{\mathrm{LH}_i})/kT] \\ & + r_{\mathrm{L}}^{\mathrm{H}} \sum_{i=1}^{12} \exp[-(\Delta^*_{\mathrm{HL}} + \varepsilon_{\mathrm{HL}_i})/kT] + r_{\mathrm{L}}^{\mathrm{H}} r_{\mathrm{L}}^{\mathrm{H}} \sum_{i=1}^{36} \exp[-(\Delta^*_{\mathrm{HH}} + \varepsilon_{\mathrm{HH}_i})/kT]\} \end{aligned} \tag{19}$$

where we introduced the effective (vibrational) degeneracy ratio for a single L → H transition

$$r_{\mathrm{L}}^{\mathrm{H}}(T)=\left[\frac{1-\exp(-h\bar{\nu}_{\mathrm{L}}/kT)}{1-\exp(-h\bar{\nu}_{\mathrm{H}}/kT)}\right]^{m} \tag{20}$$

At the same time, new energy gaps appear

$$\Delta_{\mathrm{LH}}^{*}=\Delta_{\mathrm{LH}}+(h\bar{\nu}_{\mathrm{H}}-h\bar{\nu}_{\mathrm{L}})(m/2) \tag{21}$$

$$\Delta_{\mathrm{HH}}^{*}=\Delta_{\mathrm{HH}}+(h\bar{\nu}_{\mathrm{H}}-h\bar{\nu}_{\mathrm{L}})m \tag{22}$$

In summary, we applied a fully numerical treatment based upon the eigenvalue problem of the spin-Hamiltonian matrix. The magnetic parameters entering the model are:

i. magnetogyric ratios $g_{1\mathrm{L}}$, $g_{1\mathrm{H}}$, $g_{2\mathrm{L}}$, $g_{2\mathrm{H}}$ (these collapse to g_{L} and g_{H} when LH and HL pairs are equivalent; $g_{\mathrm{H}} = 2.0$ can be fixed for the HS Fe(III) center);
ii. isotropic exchange coupling constants J_{LL}, J_{LH}, J_{HL}, J_{HH} (for equivalent LH and HL pairs, $J_{\mathrm{LH}} = J_{\mathrm{HL}}$ holds true);
iii. the (pair-interaction) asymmetric exchange parameter D_{LL} (notice, D_{L} is zero for $S = 1/2$ reference state) and eventually the (single-ion) asymmetric exchange parameter D_{H} (these are effective for low-temperature susceptibility and magnetization data when LL and HL states are populated);
iv. omitting the vibrational contribution, one can proceed with the total partition function $Z(B_r)$ consisting of 64 terms where the Δ_{LH}, Δ_{HL}, and Δ_{HH} parameters occur (with equivalent LH and HL pairs, $\Delta_{\mathrm{LH}} = \Delta_{\mathrm{HL}}$ holds true). The involvement of the vibrational contribution requires additional parameters, i.e., $h\bar{\nu}_{\mathrm{H}}$ and eventually $h\bar{\nu}_{\mathrm{L}}/h\bar{\nu}_{\mathrm{H}}$.

The minimum parameter set covers g_{L}, g_{H} (~2), J_{LL}, J_{LH} (=J_{HL}), J_{HH}, $D_{\mathrm{H}} \sim 0$, D_{LL}, $\Delta_{\mathrm{LH}} = \Delta_{\mathrm{HL}}$, Δ_{HH}, and $h\bar{\nu}_{\mathrm{H}}$. Any other simplification is unrealistic. One can argue that the parameter set is too extensive and the model overparametrized. The experience shows that simplified versions do not work properly. A single dataset (say, the temperature-dependence of the susceptibility) is surely not capable of fixing such a numerous set of parameters reliably. However, by treating three different datasets simultaneously $\{\chi = f_1(T)$, $M = f_2(B,[T])$, and $x_{\mathrm{HS}}^{(\mathrm{MS})} = f_3(T)\}$, we arrived at the minimum of the postulated functional

$$F(\ldots p_i \ldots)=\left[w_1(1/n)\sum_{n}^{N}\left|\frac{\chi_n^{\mathrm{o}}-\chi_n^{\mathrm{c}}}{\chi_n^{\mathrm{o}}}\right|\right]+\left[w_2(1/m)\sum_{m}^{M}\left|\frac{M_m^{\mathrm{o}}-M_m^{\mathrm{c}}}{M_m^{\mathrm{o}}}\right|\right]+\left[w_3(1/k)\sum_{k}^{K}\left|\frac{x_k^{\mathrm{o}}-x_k^{\mathrm{c}}}{x_k^{\mathrm{o}}}\right|\right] \tag{23}$$

by using advanced methods of nonlinear optimization (a simulated-annealing method, and genetic algorithm). Several dozens of initial trials and several thousands of optimization steps have been tested in order to identify the stationary solution. In fitting the magnetic data for the spin-crossover systems, the reference level Δ_{LL} is taken at the zero.

SPIN-CROSSOVER SYSTEMS

The complex **2a** contains nonequivalent coordination sites (Fig. 6), and thus the LH and HL states are different in energy. It is unlikely that the C-coordinated Fe(III) center (Fe1) will adopt the HS state and, at the same time, the N-coordinated site (Fe8) would be LS. Thus, the LH situation is natural, and one can assume Δ_{LH} to be small, whereas Δ_{HL} can be artificially lifted to a very high value (i.e., 10 000 K).

The magnetization (per formula unit) for **2a** taken at $T = 2.0$ K shows a progressive deviation from the value of $M_1 = M_{mol}/N_A = 2.0\ \mu_B$ assumed for the pure ground LL state (Fig. 15). It saturates to $M_1 = 3.5\ \mu_B$, which does not correspond to the pure LH state with $M_{(S=3)} = 6$. This means that both LL and LH states are populated at $T = 2.0$ K so that $\Delta_{LH}/k = 4.5$ K is a realistic estimate. The HH state lies at much higher energy, $\Delta_{HH}/k = 903$ K, which causes a weak increase of the effective magnetic moment above 150 K. This is supported by the calculated Boltzmann population factors for the HH state (bottom-right panel of Fig. 15). The value of the mean vibrational frequency refers to the wavenumber $\bar{\nu}_H = 238\ cm^{-1}$ ($\bar{\nu}_L/\bar{\nu}_H = 1.16$) which spans the experimental range known for mononuclear Fe(III) complexes. For instance, six skeletal vibrational modes for the $\{Fe^{III}N_4O_2\}$ chromophore in the HS state have been detected between 182 and 531 cm^{-1} [25]. The set of calculated magnetic and spin-crossover parameters is listed in Table 4.

Table 4 Calculated spin-Hamiltonian and spin-crossover parameters.

Parameter	**2a**	**2b**	**3a**	**3d**	**3e**
g_L	2.65	2.90	2.89	2.58	2.89
g_H	1.80	1.80	2.00	2.14	2.19
$(J_{LL}/hc)/cm^{-1}$	–3.93	–3.93	–7.62	–4.93	–0.18
$(J_{LH}/hc)/cm^{-1}$	–0.16	–31.0	–0.33	–0.13	–0.16
$(J_{HH}/hc)/cm^{-1}$	–3.67	–6.31	–0.68	–7.68	–8.67
$(D_{LL}/hc)/cm^{-1}$	–1.77	–19.3	–7.39	–6.77	–1.36
$(D_H/hc)/cm^{-1}$	–4.20	–27.0	–2.68	–3.03	–3.11
(D_{LH}/k)/K	4.51[a]	9.72[a]	1.70[b]	8.86[b]	12.5[b]
(D_{HH}/k)/K	903	300	550	554	513
$\bar{\nu}_H/cm^{-1}$	238	100	116	220	216
$\bar{\nu}_L/\bar{\nu}_H$	1.16	1.13	1.10	1.19	1.17
$R(\chi)$[c]	0.020	0.016	0.042	0.010	0.014
$R(M)$	0.022	0.059	0.052	0.055	0.046
$R(x)$	0.0006	–	0.11	–	–

[a]Fixed value $\Delta_{HL}/k = 10\,000$ K.
[b]$\Delta_{HL} = \Delta_{LH}$.
[c]$R(p)$ = conventional discrepancy factors for property p.

The energy levels of **2a** form two well-separated bands: at low temperature only the (LL + LH) manifolds interplay; the HH multiplets become populated above 120 K when the spin crossover starts being visible.

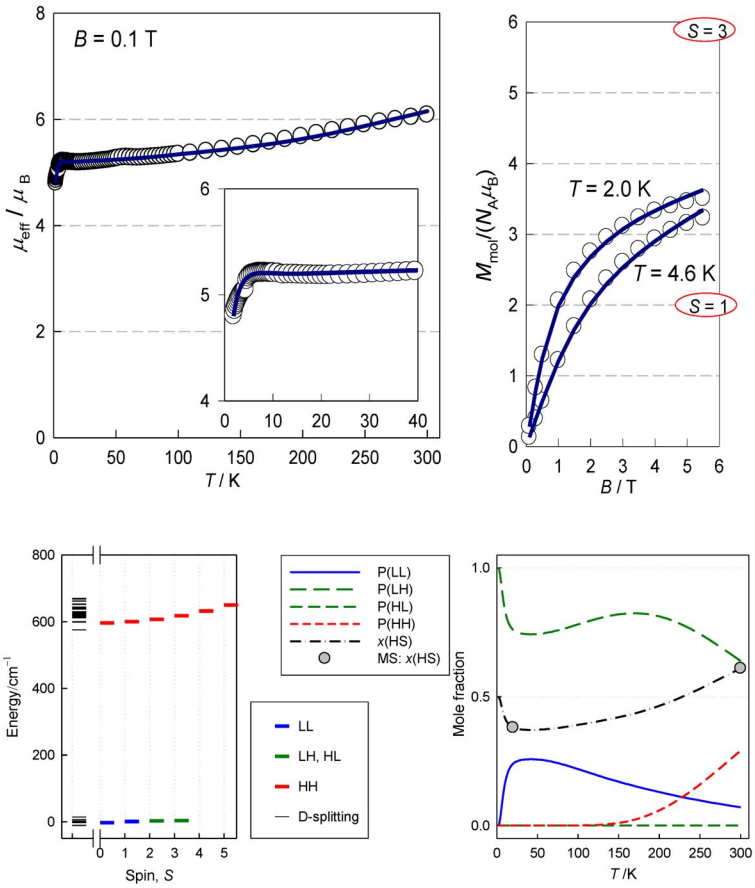

Fig. 15 Magnetic data for dinuclear complex **2a**, [(*salpet*)Fe{CN}Fe(*salpet*)]ClO_4·$2H_2O$. Solid lines: fitted data. Classification: B/LL+LH group. Bottom left: reconstructed energy levels; bottom right: Boltzmann population factors for individual reference states, HS mole fraction (dot-dashed), and Mössbauer data (filled points).

Watching the low-temperature effective magnetic moment for **2b**, one could conclude that the LL pair alone is present as a ground state (Fig. 16). However, the magnetization (per formula unit) taken at $T = 2.0$ K shows a substantial deviation from the value of $M_1 = M_{mol}/N_A = 2.0\ \mu_B$ assumed for the pure ground LL state: it saturates only to $M_1 = 1.27\ \mu_B$ at $B = 7$ T. This feature indicates a presence of either very strong asymmetric or eventually antisymmetric exchange. Indeed, the $(J + D)$-splitting causes the energy levels to form a broad band after the first energy gap; its Boltzmann population results in a gradual spin crossover.

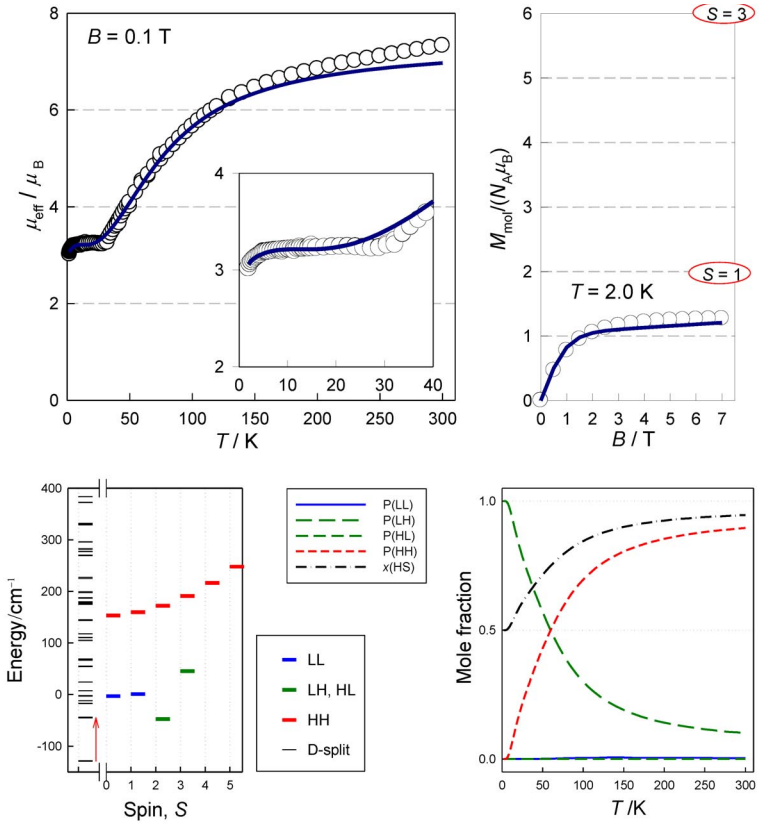

Fig. 16 Magnetic data for dinuclear complex **2b**, [Fe(MeBu-*salpet*){CN}Fe(MeBu-*salpet*)][BPh_4]·2CH_3CN. Solid lines: fitted data. Classification: B/LL+LH group. Bottom left: reconstructed energy levels; bottom right: Boltzmann population factors for individual reference states, and HS mole fraction (dot-dashed).

The trinuclear complex **3a** consists of a diamagnetic central unit {$Fe^{II}(CN)_5(NO)$}. The magnetic data measured carefully until $T = 350$ K reveal that at the highest temperature $\mu_{eff} \sim 7.7\ \mu_B$, whereas at $T = 4$ K $\mu_{eff} \sim 6.0\ \mu_B$ holds true (Fig. 17). The magnetization at $T = 2.0$ K is $M_{mol}/N_A = 4.5\ \mu_B$, indicating that in addition to the LL state the LH (=HL) is also populated. Thus, $E_{LL} \sim E_{LH} = E_{LH} << E_{HH}$ needs to be fulfilled for the reference states. The magnetic data are in harmony with the MS, showing that a kind of spin crossover proceeds: at $T = 20$ K, the renormalized area fraction is 0.45 for Fe(III)-HS, and at $T = 300$ K this is 0.75.

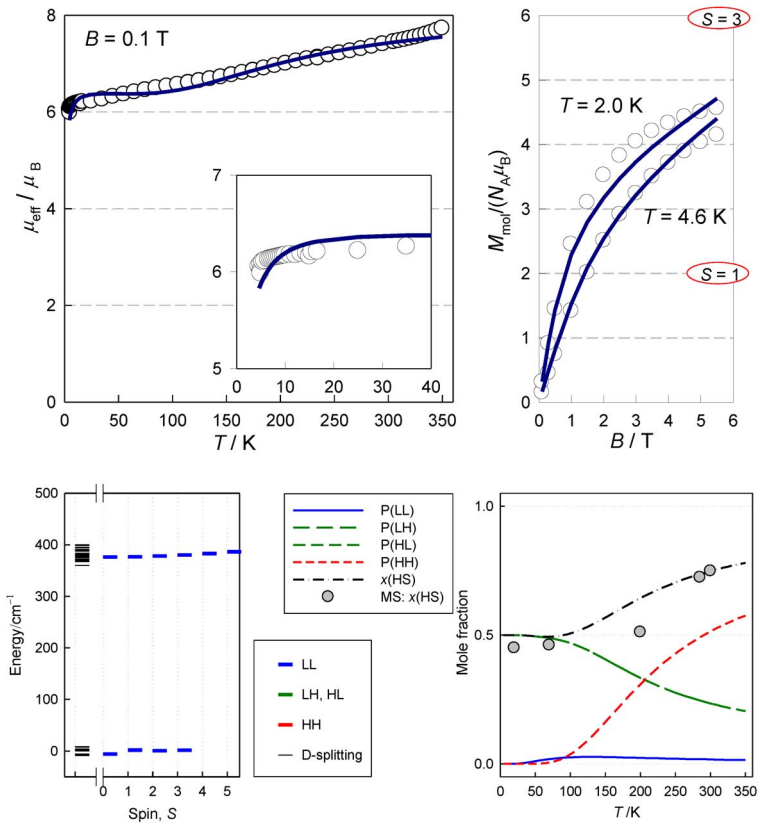

Fig. 17 Magnetic data for the trinuclear complex **3a**, $[\{Fe^{II}(CN)_5(NO)\}\{Fe^{III}(salpet)\}_2]\cdot 3.65H_2O$. Full lines: fitted data. Classification: B/LL+LH group. Bottom left: reconstructed energy levels; bottom right: Boltzmann population factors for individual reference states, HS mole fraction (dot-dashed), and Mössbauer data (filled points).

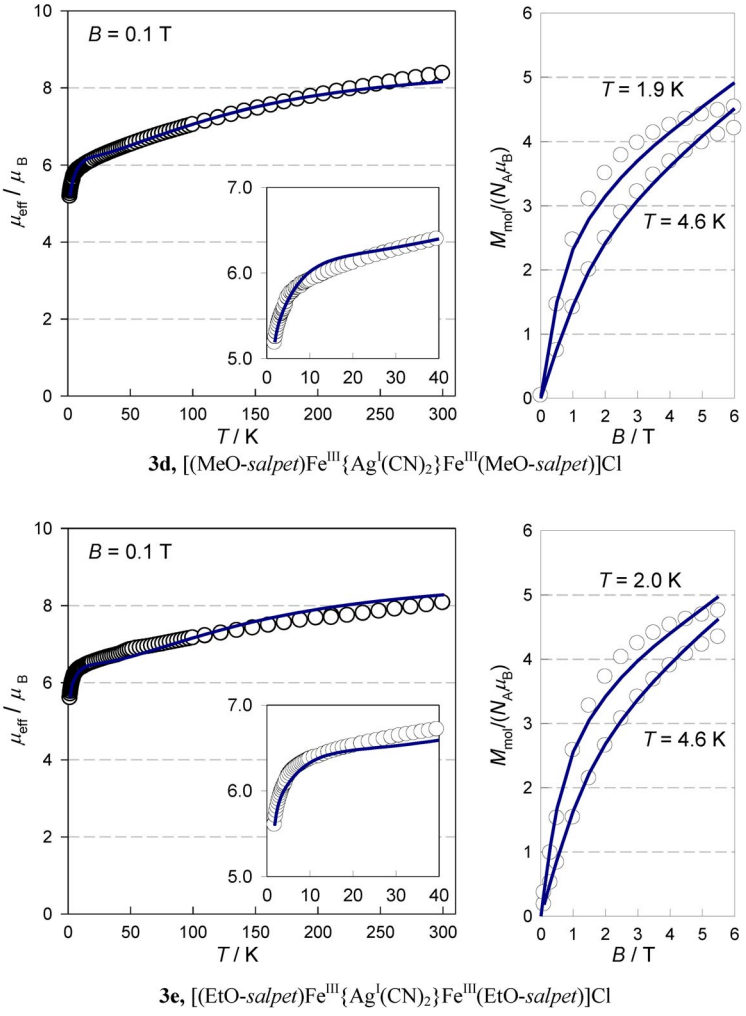

Fig. 18 Magnetic data for the trinuclear complexes **3d** and **3e**. Left: temperature dependence of the effective magnetic moment; right: field dependence of the magnetization. Open circles: experimental data, solid lines: fitted.

CONCLUSIONS

In dinuclear systems, the reference electron configurations (LL, LH, HA, and HH) could be close in their energy. Weak exchange interaction manifests itself in forming the energy bands (made of magnetic energy levels), which could be mutually overlapped. Therefore, the spin crossover in dinuclear (polynuclear) systems can be influenced by the magnetic exchange interaction (Fig. 19).

When the ground reference state is LL, but HL (LH) or HH states are close in energy (classification: group B/LL), the thermally induced spin crossover is very gradual. Even at very low temperature, in addition to the LL spin-multiplets, LH ones are also populated, and the system exhibits an increased magnetic productivity (measured by the product χT, or effective magnetic moment μ_{eff}). This causes a behavior improperly termed as "residual HH fraction" or "incomplete spin transition".

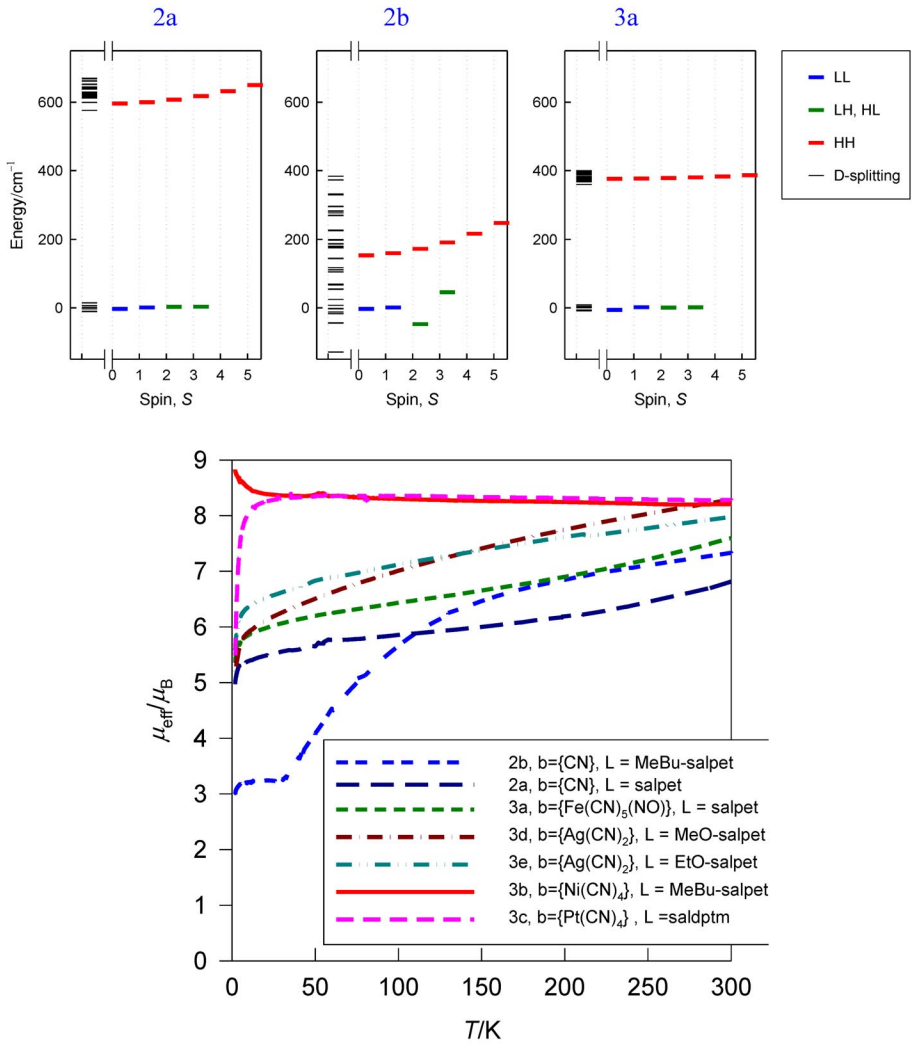

Fig. 19 Comparison of magnetic data for spin crossover and HS dinuclear and trinuclear complexes linked by a diamagnetic bridge b.

ACKNOWLEDGMENTS

Grant agencies (Slovakia: VEGA 1/0213/08, APVV 0006-07, COST-0006-06, VVCE 0004-07, APVV-Stefanik; Germany: DFG SPP 1137 Re1627/1-3, Leibniz UNI; Czech Republic: MSM6198959218; ESF: COST-D35) are acknowledged for the financial support. Prof. J. Linares (University of Versailles, France) is acknowledged for scanning a part of the MS.

REFERENCES

1. R. Boča, W. Linert. *Monatsh. Chem.* **134**, 199 (2003).
2. O. Kahn. *Molecular Magnetism*, VCH, New York (1993).
3. R. Boča. *Struct. Bonding* **117**, 1 (2006).
4. P. Gütlich, H. A. Goodwin (Eds.). *Spin Crossover in Transition Metal Compounds*, Vols. I–III, in Topics in Current Chemistry, Vols. 233–235, Springer (2004).

5. S. Brooker, P. G. Plieger, B. Moubaraki, K. S. Murray. *Angew. Chem., Int. Ed*. **38**, 408 (1999).
6. R. Boča, Y. Fukuda, M. Gembický, R. Herchel, R. Jaroščiak, W. Linert, F. Renz, J. Yuzurihara. *Chem. Phys. Lett*. **325**, 411 (2000).
7. V. Ksenofontov, A. B. Gaspar, J. A. Real, P. Gütlich. *J. Phys. Chem.* **B105**, 12266 (2001).
8. V. Ksenofontov, H. Spiering, S. Reiman, Y. Garcia, A. B. Gaspar, N. Moliner, J. A. Real, P. Gütlich. *Chem. Phys. Lett*. **348**, 381 (2001).
9. A. B. Gaspar, V. Ksenofontov, M. Seredyuk, P. Gütlich. *Coord. Chem. Rev*. **249**, 2661 (2005).
10. A. B. Gaspar, M. C. Munoz, J. A. Real. *J. Mater. Chem.* **16**, 2522 (2006).
11. R. Herchel, R. Boča, M. Gembický, J. Kožíšek, F. Renz. *Inorg. Chem*. **43**, 4103 (2004).
12. E. Breuning, M. Ruben, J.-M. Lehn, F. Renz, Y. Garcia, V. Ksenofontov, P. Gütlich, E. Wegelius, K. Rissanen. *Angew. Chem., Int. Ed*. **39**, 2504 (2000).
13. M. Nihei, M. Ui, M. Yokota, L. Han, A. Maeda, H. Kishida, H. Okamoto, H. Oshio. *Angew. Chem., Int. Ed*. **44**, 6484 (2005).
14. R. Boča, I. Šalitroš, J. Kožíšek, J. Linares, J. Moncoľ, F. Renz. Submitted for publication.
15. F. Renz, P. Kerep. *Polyhedron* **24**, 2849 (2005).
16. F. Renz, D. Hill, M. Klein, J. Hefner. *Polyhedron* **26**, 2325 (2007).
17. I. Šalitroš, R. Boča, Ľ. Dlháň, M. Gembický, J. Kožíšek, J. Linares, J. Moncoľ, I. Nemec, L. Perašínová, J. Pavlik, F. Renz, I. Svoboda, H. Fuess. *Eur. J. Inorg. Chem.* 3141 (2009).
18. E. M. Holt, S. L. Holt, M. Vlasse. *Cryst. Struct. Commun*. **8**, 645 (1979).
19. G. Rogez, A. Marvilliers, P. Sarr, S. Parsons, S. J. Teat, L. Ricard, T. Mallah. *Chem. Commun*. 1460 (2002).
20. R. Boča. *Theoretical Foundations of Molecular Magnetism*, Elsevier, Amsterdam (1999).
21. J.-A. Real, H. Bolvin, A. Bousseksou, A. Dworkin, O. Kahn, F. Varret, J. Zarembowitch. *J. Am. Chem. Soc.* **114**, 4750 (1992).
22. A. Bousseksou, F. Varret, J. Nasser. *J. Phys. I* **3**, 1463 (1993).
23. A. Bousseksou, H. Constant-Machado, F. Varret. *J. Phys. I* **5**, 747 (1995).
24. R. Boča, M. Boča, L. Dlháň, K. Falk, H. Fuess, W. Haase, R. Jaroščiak, B. Papánková, F. Renz, M. Vrbová, R. Werner. *Inorg. Chem.* **40**, 3025 (2001).
25. K. Kaji, M. Sorai, A. J. Conti, D. N. Hendrickson. *J. Phys. Chem. Solids* **54**, 1621 (1993).